SCIENCE CHINA
Information Sciences

• RESEARCH PAPER •

June 2021, Vol. 64 162403:1–162403:19
https://doi.org/10.1007/s11432-020-3100-8

Detection of the interictal epileptic discharges based on wavelet bispectrum interaction and recurrent neural network

Nabil SABOR[1,2,3*], Yongfu LI[1,2], Zhe ZHANG[1,2], Yu PU[4], Guoxing WANG[1,2*] & Yong LIAN[1,2]

[1]*Department of Micro-Nano Electronics, Shanghai Jiao Tong University, Shanghai* 200240*, China;*
[2]*MoE Key Lab of Artificial Intelligence, Shanghai Jiao Tong University, Shanghai* 200240*, China;*
[3]*Electrical Engineering Department, Assiut University, Assiut* 71516*, Egypt;*
[4]*Alibaba DAMO Academy, Sunnyvale* CA 94085*, USA*

Received 5 May 2020/Revised 9 July 2020/Accepted 3 September 2020/Published online 27 April 2021

Abstract Detection of interictal epileptic discharges (IED) events in the EEG recordings is a critical indicator for detecting and diagnosing epileptic seizures. We propose a key technology to extract the most important features related to epileptic seizures and identifies the IED events based on the interaction between frequencies of EEG with the help of a two-level recurrent neural network. The proposed classification network is trained and validated using the largest publicly available EEG dataset from Temple University Hospital. Experimental results clarified that the interaction between β and β bands, β and γ bands, γ and γ bands, δ and δ bands, θ and α bands, and θ and β bands have a significant effect on detecting the IED discharges. Moreover, the obtained results showed that the proposed technique detects 95.36% of the IED epileptic events with a false-alarm rate of 4.52% and a precision of 87.33% by using only 25 significant features. Furthermore, the proposed system requires only 164 ms for detecting a 1-s IED event which makes it suitable for real-time applications

Keywords interictal epileptic discharges, epilepsy, discrete wavelet transform, wavelet bispectrum, long short-term memory, recurrent neural network

Citation Sabor N, Li Y F, Zhang Z, et al. Detection of the interictal epileptic discharges based on wavelet bispectrum interaction and recurrent neural network. Sci China Inf Sci, 2021, 64(6): 162403, https://doi.org/10.1007/s11432-020-3100-8

1 Introduction

Epilepsy is the fourth most commonly known neurological disease in the world according to the latest data from the World Health Organization [1]. It can threaten the patients' lives with brain failure, heart and lung failure, head trauma, and sudden unexpected death [2]. The diagnosis and treatment of epilepsy in hospitals depend on detecting the interictal epileptic discharges (IED) of EEG recordings and calculating the IED index. The detection of IED is a difficult task because some IED events may easily be overshadowed by large EEG background, eye movement or artifacts. In addition, varying spike morphology during the sleep cycle for long-term monitoring increases the difficulty of detecting the IED discharges. The visual analysis and scoring of the IED events from EEG require experienced neurophysiologists and are very time-consuming processes, especially in the case of long-term recordings, and subject to observer error [3]. Hence, developing an automatic system for detecting IED can help for diagnosing and saving the lives of epileptic patients and also saves the time of neurophysiologists. The developed system should be multi-modal, low power, flexible, and has a high precision to satisfy the clinicians' requirements by detecting all IED discharges of EEG recording with small false positive detections (i.e., sensitivity above 95% and a false alarm rate below 5%) [4–8]. The challenge is how to tradeoff between the sensitivity and the false alarm rate to improve the system precision.

* Corresponding author (email: nabil_sabor@aun.edu.eg, guoxing@sjtu.edu.cn)

Table 1 State-of-the-art methods for detection of epileptic IED discharges

Method	Dataset	Dataset availability	Features method	Features type	Classifier	ACC (%)	SEN (%)	SPE (%)	FPR	PREC (%)	F1-score (%)	Gmean (%)
Zacharaki et al. [3]	One-subject with 101 spikes (2 channels)	NO	Locality preserving projections (LPP)	Amplitude-based	Support vector machine (SVM)	–	97	98.74	1.26%	62.8	76.24	97.87
Golmohammedi et al. [8]	Publicly largest TUH EEG dataset (390 subjects, 22 channels)	Yes	Hidden Markov models (HMM)	–	Deep l earning	–	90.1	95.11	4.89%	–	–	92.6
Carey et al. [9]	6 patients (one-channel)	NO	–	–	Artificial neural network (ANN)	–	82.68	–	–	72.7	77.37	–
Lodder et al. [10]	23 patients with 723 IEDs	NO	Template matching	Amplitude-based	SVM	–	90	–	2.36 (min)	23.10	36.76	–
Malik et al. [11]	13 subjects	NO	Gradient-based NEO	Amplitude-based	–	74.1	–	–	–	–	–	–
Liu et al. [13]	12 epileptic patients (16 channels)	NO	–	Morphological-based	AdaBoost	93.9	95.5	92.4	7.6%	–	–	93.94
Douget et al. [14]	17 subjects (3 channels)	NO	Discrete wavelet transform (DWT)	Wavelet coefficient-based	Random forest	–	62	–	–	26	36.64	–
Antonio et al. [15]	two-subjects with 96 spikes	NO	Cross-correlation	Amplitude-based	Decision tree	97	86	98	2%	–	–	91.80

*ACC: accuracy, SEN: sensitivity, SPE: specificity, FPR: false positive rate or false alarm rate, PREC: precision, Gmean: geometric mean.

Many methods have been developed for detecting the IED discharge events from the EEG recordings as listed in Table 1. It is observed that most of the state-of-the-art methods [3, 8–15] did not satisfy the clinicians' requirements. The method in [3] meets the clinicians' requirements. However, it is based on only one subject. Also, most methods extracted features from changes in the amplitude of the EEG signal which is varied during the sleep cycle. Epilepsy originates from recurrent abnormal discharges of the brain's electrical activity. These epileptic discharges lead to the subtle changes in the frequencies of the EEG signal. This prompts us to study the interaction between frequencies of the EEG signal to track the changes in EEG arising from linear and nonlinear changes under a variety of physiologic conditions. Recently, the higher-order statistic (HOS) methods [16–21] such as bispectrum (BS) and wavelet bispectrum (WBS) have been used for extracting features of the bio-signals. HOS methods explore the existence of quadratic (and cubic) nonlinear coupling between the different frequency components of a signal. In contrast to the traditional power spectrum, HOS analysis preserves the phase information and detects the nonlinearity and deviation from Gaussianality of the non-stationary signals.

Due to features of HOS techniques for the non-stationary signals, we propose an automatic system for detecting epileptic events based on studying the interaction between the frequencies of EEG recordings using the WBS method with a combination of recurrent neural network (RNN). Also, selecting a minimum number of features and optimizing the classification network will be considered to reduce the complexity of the proposed system and make it a low power system. The proposed system is trained and tested using the largest publicly available EEG dataset of Temple University Hospital (TUH) [22] for classifying the EEG signal into six different events as three epileptic events and three background events. The main contributions of this paper can be summarized as follows:

• Proposed a key technology for extracting features based on the interaction among frequency-bands of the EEG's events by combining DWT and WBS techniques.

• Proposed a two-level classification network using an RNN architecture based on a long short-term memory (LSTM) for tracking features changing over time and classifying the extracted features into the different events with an average accuracy of 95.45%.

The paper is organized as follows. The detail of the EEG TUH dataset is presented in Section 2. Section 3 describes the details of the proposed IED detection system. In Section 4, the obtained results are explained. Section 5 offers some conclusions and future work.

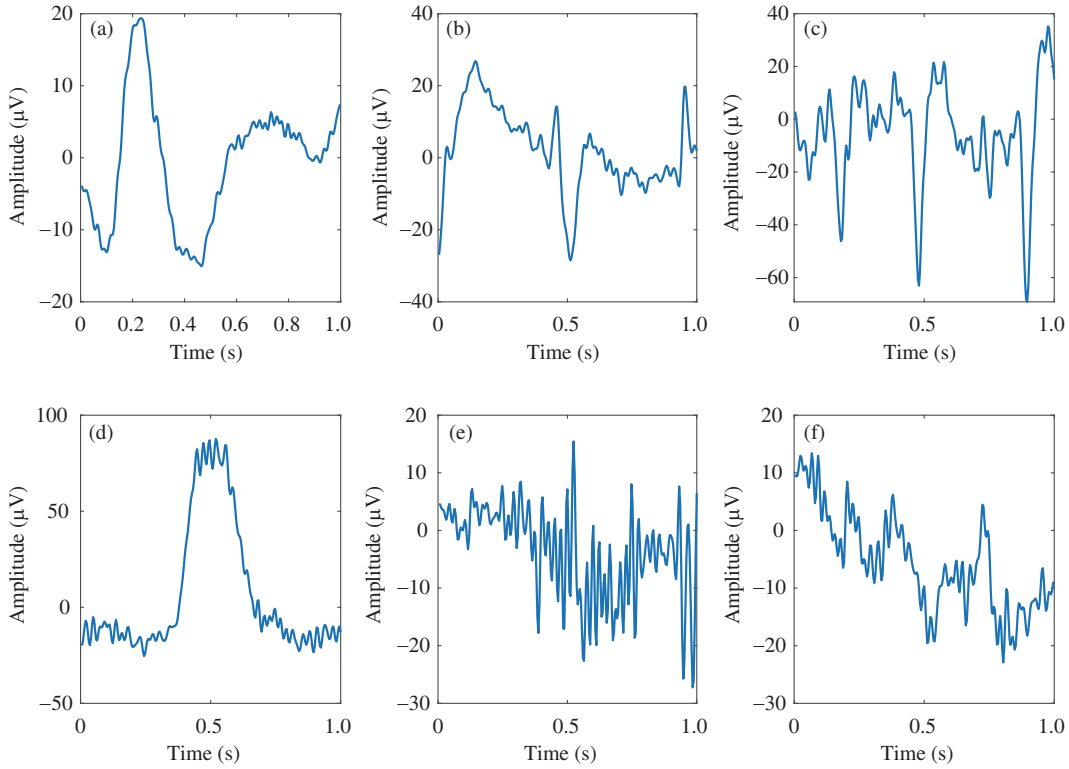

Figure 1 (Color online) Six events of TUEV EEG dataset. (a) SPSW; (b) GPED; (c) PLED; (d) EYEM; (e) ARTF; (f) BCKG.

Table 2 Distribution of EEG's events in the TUEV EEG dataset

Event	Training set		Testing set	
	Count	Percentage (%)	Count	Percentage (%)
SPSW	645	0.91	567	1.93
GPED	7050	9.54	4677	15.9
PLED	4120	5.58	1998	6.79
EYEM	940	1.27	329	1.12
ARTF	9329	12.63	2204	7.49
BCKG	51790	70.11	19646	66.78
Total	**73874**	**100**	**29421**	**100**

2 Dataset

According to the state-of-the-art method mentioned in Table 1, all methods used their dataset except [8] used the publicly TUH dataset. The TUH is the only available annotated spike dataset, so we used it in this study. The TUH dataset contains over 30000 sessions from over 16000 patients collected from the Department of Neurology at Temple University Hospital. These EEG recordings were recorded using several generations of Natus Medical Incorporated's Nicolet^{TM} EEG recording technology with the 10/20 international electrode placement method. The sampling frequency of the raw EEG varies between 256 Hz and 1 kHz and the number of channels in each recording varies between 20 and 128 channels. The EEG recordings are given in an averaged reference (AR) montage. A portion of TUH-EEG data (390 patients), called TUEV dataset, was annotated manually at the TUH Hospital into six 1-s epileptic events as shown in Figure 1, namely spike and/or sharp waves (SPSW), periodic lateralized epileptiform discharges (PLED), generalized periodic epileptiform discharges (GPED), eye movement (EYEM), artifacts (ARTF), and background (BCKG). The annotation of the six events is given for the two common reference points (TCP) montage [23]. Hence, all EEG recordings should be converted to 22 channels TCP montage and are resampled at 250 Hz. The distribution of the six 1-s events in both the training and the testing sets is given in Table 2. The total duration of all events in both training and testing sets is 28.69 h.

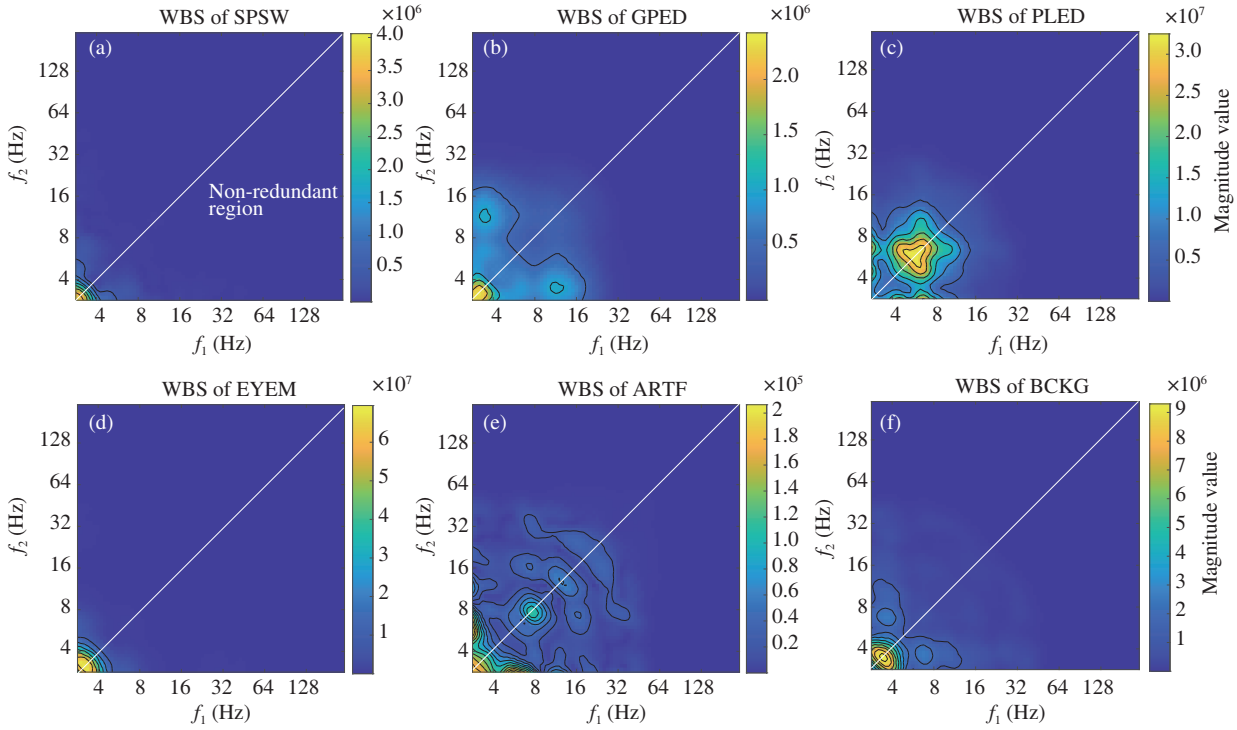

Figure 2 (Color online) Auto-interactions of the whole frequency range of six different IED events using the WBS method. (a) SPSW; (b) GPED; (c) PLED; (d) EYEM; (e) ARTF; (f) BCKG.

3 The proposed detection system

The development of a high precision system for detecting the IED discharges mainly depends on the extracted features and the classification network. This paper proposes a key technology for extracting accurate features based on studying the interactions between frequencies of EEG recordings. Figure 2 shows the interaction between the whole frequency range of the different six events shown in Figure 1 using the WBS method. It is observed that the WBS of SPSW and GPED events are similar and have one peak at frequencies below 4 Hz, but GPED has some high-level values within frequencies 4 to 32 Hz as compared to SPSW. The WBS of the EYEM event is similar to that of the SPSW event, but the magnitude of the peak is high. Also, we can observe that SPSW and BCKG events have similar WBS. This means that exploring the whole frequency range may not enough to distinguish between the different events.

The study of the interaction among different frequency-bands (δ, θ, α, β, and γ) using the WBS method gives valuable details for distinguishing between different events as shown in Figure 3. It is seen that zones of the highest interaction obtained in WBS of different frequency-bands have different values and shapes and occurred at different locations for each event. The $\mathrm{WBS}_{\gamma\gamma}$ of SPSW has three high interaction zones, while the GPED has a wide interaction zone in the $\mathrm{WBS}_{\delta\delta}$. PLED has the highest interaction zone around 8 Hz in the $\mathrm{WBS}_{\alpha\alpha}$. At 10 Hz, there is a high interaction zone in the $\mathrm{WBS}_{\alpha\alpha}$ of the EYEM event. Two interaction zones at frequencies 28 Hz and 48 Hz in the $\mathrm{WBS}_{\gamma\gamma}$ of ARTF. While in BCKG event, the $\mathrm{WBS}_{\alpha\alpha}$ and the $\mathrm{WBS}_{\beta\beta}$ have distinguishable shapes. This means that the interaction between frequency-bands of the EEG signal is more effective than exploring the whole frequency for distinguishing between the considered events. To characterize each event, we need to measure the magnitude and location of the interaction zone, the power distribution, the energy, and the regularity of each WBS. In this study, 12 linear and non-linear features are computed from the bispectrum domain in addition to 10 features that are calculated from the time domain to measure the morphology shape of each event. These features are discussed late in this section.

The challenge of detecting IED is isolating the epileptic events from the EEG background. It is not efficient to classify all epileptic and background events at the same time. We propose a two-level classification network for reducing the problem of imbalanced data of the different events. The first-

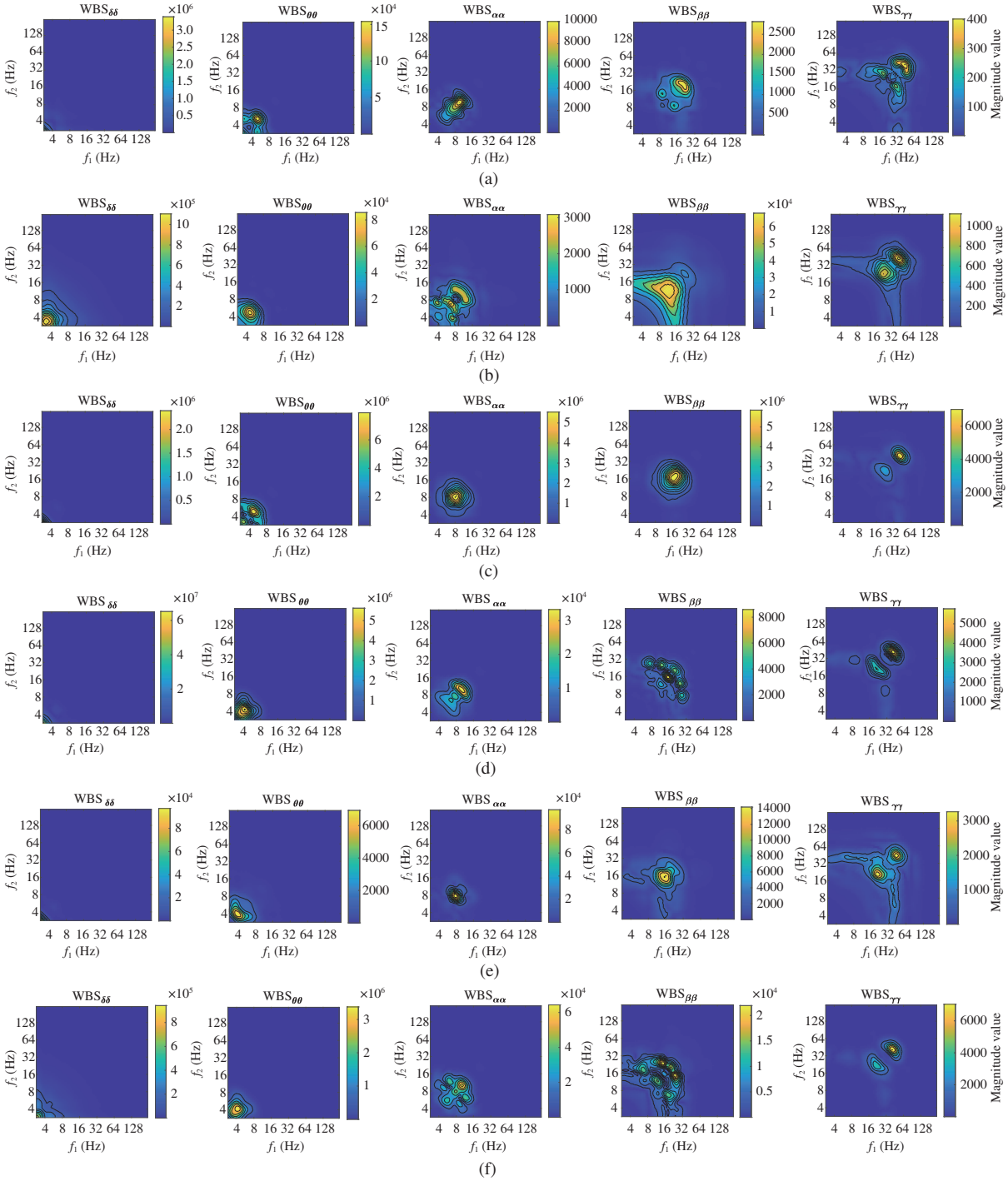

Figure 3 (Color online) Auto-interactions of six different IED events using the WBS method: rows represent the interactions of five frequency-bands of (a) SPSW, (b) GPED, (c) PLED, (d) EYEM, (e) ARTF, and (f) BCKG respectively, while columns represent the interactions between δ vs. δ, θ vs. θ, α vs. α, β vs. β, and γ vs. γ respectively.

level concerns on classifying data into epileptic and non-epileptic events by grouping training data of all events into epileptic class and non-epileptic class. This allows us to isolate the epileptic events from the background events which is the main issue for diagnosing epileptic seizures. After that, the second classification level uses two 3-way classifiers for classifying the epileptic waves into SPSW, PLED, and GPED events and the non-epileptic waves into EYEM, ARTF, and BCKG events. Figure 4 shows the block diagram of the proposed system. Firstly, the EEG recordings are filtered using an infinite impulse response (IIR) elliptic bandpass filter with cutoff frequencies [0.5 49] Hz to remove the unwanted

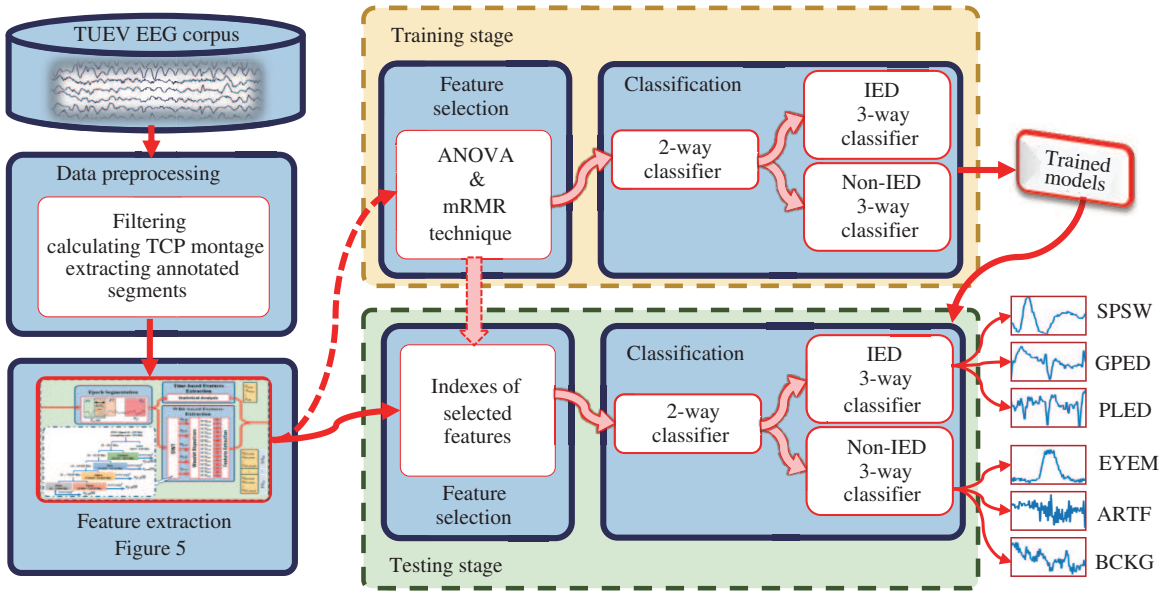

Figure 4 (Color online) Block diagram of the proposed system for detecting the epileptic IED discharges. The proposed system consists of four steps, namely data preprocessing, feature extraction, feature selection and classification.

Table 3 Time-domian based features[a)]

Number	Feature	Equation	Number	Feature	Equation
1	Mean of absolute value	$X_{\text{avg}} = \frac{1}{N}\sum_{n=1}^{N}\lvert x_f\rvert$	6	Kurtosis of data	$X_{\text{kurt}} = \frac{1}{NX_\sigma^4}\sum_{n=1}^{N}(\lvert x_f - \mu_x\rvert)^4$
2	Maximum value	$X_{\max} = \max(x_f)$	7	Hjorth mobility	$X_{\text{mob}} = \text{mob}(x_w(n)) = \sqrt{\left(\frac{\text{var}(x'_f)}{\text{var}(x_f)}\right)}$
3	Sum of logarithmic amplitude	$X_{\text{slog}} = \sum_{n=1}^{N}\lvert x_f\rvert$	8	Hjorth complexity	$X_{\text{comp}} = \frac{\text{mob}(x'_f)}{\text{mob}(x_f)}$
4	Variance of data	$X_\sigma = \text{var}(x_w(n) = \frac{1}{N}\sum_{n=1}^{N}(\lvert x_f - \mu_x\rvert)^2$	9	Fractal dimension index	$X_{\text{FD}} = \frac{\log_{10}(N-1)}{\log_{10}(d/L)+\log_{10}(N-1)}$
5	Skewness of data	$X_{\text{skew}} = \frac{1}{NX_\sigma^3}\sum_{n=1}^{N}(\lvert x_f - \mu_x\rvert)^3$	10	Sample entropy	$X_{\text{SE}} = -\log(A/B)$

a) N is the length of x_f, L is the total length along x_f, d is the distance between the first point in x_f and the point that gives the maximum distance and $\mu_x = \frac{1}{N}\sum_{n=1}^{N} x_f$ is the mean of x_f. A and B are number of pairs having distance less than tolerance (r) for $m+1$ and m matches of x_f.

frequencies, baseline wander, and power line noise (50 Hz). Then, different features are extracted from the labeled segments and passed to the classification network are shown in Figure 4.

3.1 Feature extraction

Spike and sharp waves occur in the region where seizures originate by producing an abrupt change in polarity over several milliseconds. The duration of a spike-wave is between 20 and 70 ms, while a sharp wave lasts between 70 and 200 ms. PLED events are repetitive periodic, focal, or hemispheric epileptiform discharges like sharp waves and spike waves, at intervals of between 0.5 and 3 s. GPED can be periodic short or long-interval diffuse discharges or suppression-burst patterns. To monitor the narrow transients of the epileptic discharges within 1-s epoch and extract accurate features, each 1-s epoch is divided into f_r frames (timesteps) $(x_f(i),\ i = 1, 2, \ldots, f_r)$ using a T_w-s window with 50% overlapping as shown in Figure 5. For each frame, different time- and bispectrum-based features are extracted.

3.1.1 *Time-domain based features*

The time-domain based features are calculated by applying statistical analysis to each frame signal x_f. Ten features are considered to measure characteristics of the spike morphology in the time-domain. These features are the mean of absolute value, maximum value, sum of logarithmic amplitude values, variance, skewness, kurtosis, Hjorth mobility and complexity, fractal dimension index [24], and sample entropy [25] as listed in Table 3.

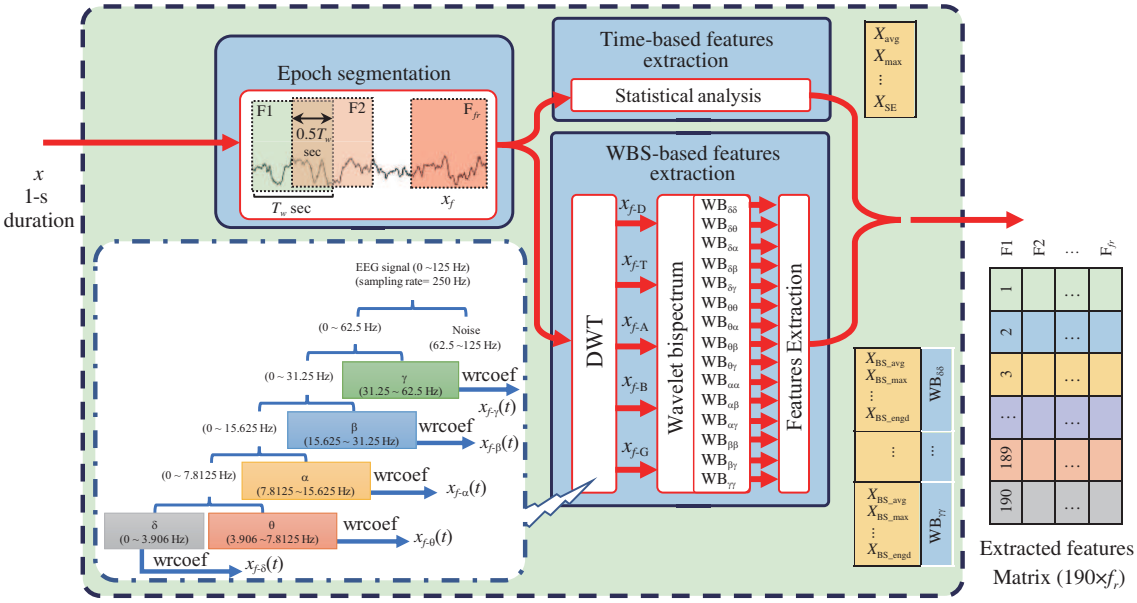

Figure 5 (Color online) Feature extraction of the proposed system. The first step is segmenting the 1-s epoch into multiple timesteps (frames), then each timestep is decomposed into five bands and the WBS among the different bands are calculated. 180 features are calculated from the obtained 15 bispectrums and 10 features are extracted from the time domain.

3.1.2 *Bi-frequency-domain based features*

As illustrated in Figure 5, the DWT [26,27] is utilized with db4 wavelet function and 5 decomposition levels to decompose the EEG signal of each frame x_f into the five frequency-bands. The signals of the different bands are reconstructed from the wavelet domain (wrcoef) to the time-domain, namely δ ($x_{f\text{-}\delta}$), θ ($x_{f\text{-}\theta}$), α ($x_{f\text{-}\alpha}$), β ($x_{f\text{-}\beta}$), and γ ($x_{f\text{-}\gamma}$) signals. The WBS method is used for calculating the auto-interaction of each band signal and the cross-interaction between the different band signals. As a result, 15 bispectrums are formed from the relation of different bands, namely 5 auto-bispectrums $\{\mathrm{WB}_{\delta\delta}, \mathrm{WB}_{\theta\theta}, \mathrm{WB}_{\alpha\alpha}, \mathrm{WB}_{\beta\beta}, \mathrm{WB}_{\gamma\gamma}\}$, and 10 cross-bispectrums $\{\mathrm{WB}_{\delta\theta}, \mathrm{WB}_{\delta\alpha}, \mathrm{WB}_{\delta\beta}, \mathrm{WB}_{\delta\gamma}, \mathrm{WB}_{\theta\alpha}, \mathrm{WB}_{\theta\beta}, \mathrm{WB}_{\theta\gamma}, \mathrm{WB}_{\alpha\beta}, \mathrm{WB}_{\alpha\gamma}, \mathrm{WB}_{\beta\gamma}\}$. For each WBS, 12 linear and non-linear features are computed to extract the quantitative and regularity information from the non-redundant region as follows:

(a) Mean magnitude of bispectrum:

$$X_{\text{BS-avg}} = \frac{1}{L}\sum_{\Omega} |\mathrm{WB}(a_1, a_2)|, \tag{1}$$

where L is the number of points in the non-redundant region (Ω), and $\mathrm{WB}(a_1, a_2)$ represents the WBS matrix.

(b) Maximum magnitude of bispectrum:

$$X_{\text{BS-max}} = \max(|\mathrm{WB}(a_1, a_2)|). \tag{2}$$

(c) Location of the maximum magnitude of bispectrum:

$$X_{\text{BS-loc}} = \mathrm{loc}(\max(|\mathrm{WB}(a_1, a_2)|)). \tag{3}$$

(d) Sum of the squared magnitude of bispectrum:

$$X_{\text{BS-eng}} = \sum_{\Omega} |\mathrm{WB}(a_1, a_2)|^2. \tag{4}$$

(e) Skewness of magnitude bispectrum:

$$X_{\text{BS-skew}} = \frac{1}{(L-1)\sigma_s^3}\sum_{\Omega} (\mathrm{WB}(a_1, a_2) - \mu_s)^3, \tag{5}$$

$$\sigma_s = \frac{1}{L}\sum_{\Omega}(\mathrm{WB}(a_1,a_2)-\mu_s)^2, \quad \mu_s = \frac{1}{L}\sum_{\Omega}\mathrm{WB}(a_1,a_2), \tag{6}$$

where μ_s and σ_s are the mean and the variance of the WBS.

(f) Kurtosis of magnitude bispectrum:

$$X_{\text{BS-kurt}} = \frac{1}{(L-1)\sigma_s^4}\sum_{\Omega}(\mathrm{WB}(a_1,a_2)-\mu_s)^4. \tag{7}$$

(g) Phase entropy:

$$X_{\text{BS-Pe}} = \sum_m p(\psi_m)\log(p(\psi_m)), \tag{8}$$

$$p(\psi_m) = \frac{1}{L}\sum_{\Omega} I(\phi(\mathrm{WB}(a_1,a_2)) \in \psi_m), \tag{9}$$

$$\psi_m = \phi| -\pi + \frac{2\pi m}{M} \leqslant \phi \leqslant -\pi + \frac{2\pi(m+1)}{M},\ m = 0,1,\ldots,M-1, \tag{10}$$

where, ϕ is the phase angle of the bispectrum, $I(\phi)$ is an indicator function that gives 1 when the value of ϕ is within the range of bin ψ_m, and M is the number of bins for ψ_m.

(h) Normalized bispectrum entropy:

$$X_{\text{BS-ent1}} = -p_n\log(p_n), \text{ where } p_n = \frac{|\mathrm{WB}(a_1,a_2)|}{\sum_{\Omega}|\mathrm{WB}(a_1,a_2)|}. \tag{11}$$

(i) Normalized bispectrum squared entropy:

$$X_{\text{BS-ent2}} = -p_s\log(p_s), \text{ where } p_s = \frac{|\mathrm{WB}(a_1,a_2)|^2}{\sum_{\Omega}|\mathrm{WB}(a_1,a_2)|^2}. \tag{12}$$

(j) Normalized bispectrum cubic entropy:

$$X_{\text{BS-ent3}} = -p_c\log(p_c), \text{ where } p_c = \frac{|\mathrm{WB}(a_1,a_2)|^3}{\sum_{\Omega}|\mathrm{WB}(a_1,a_2)|^3}. \tag{13}$$

(k) First-order spectral moment of the magnitude of diagonal elements:

$$X_{\text{BS-FOSM}} = \sum_{K=1}^{N} K\log(|\mathrm{WB}(a_K,a_K)|). \tag{14}$$

(l) Sum of the squared magnitude of diagonal elements:

$$X_{\text{BS-engdiag}} = \sum_{K=1}^{N}|\mathrm{WB}(a_K,a_K)|^2. \tag{15}$$

As a result, a $190 \times f_r$ features matrix is extracted at f_r timesteps. These features are normalized using z-score [28] to have zero mean and standard deviation of 1. Since not all extracted features are significant, the one-way ANOVA test is used to study the significance of the extracted features. The significant features should have p values less than 0.05. Then, the minimum redundancy maximum relevance (mRMR) technique [29] uses the mutual information criteria to give a high rank for features that have minimum redundant and maximum relevance to the target output. Since the number of features affects the complexity and the performance of the system, we will explain this effect in Subsection 3.2.3.

3.2 Classification network

As the IED are transient events in the EEG signal and their morphological change over time, the LSTM [30] is considered for tracking the features of these events at different timesteps and detecting their variations over time. LSTM is a specific type of RNN [31,32] architecture. A two-level classification

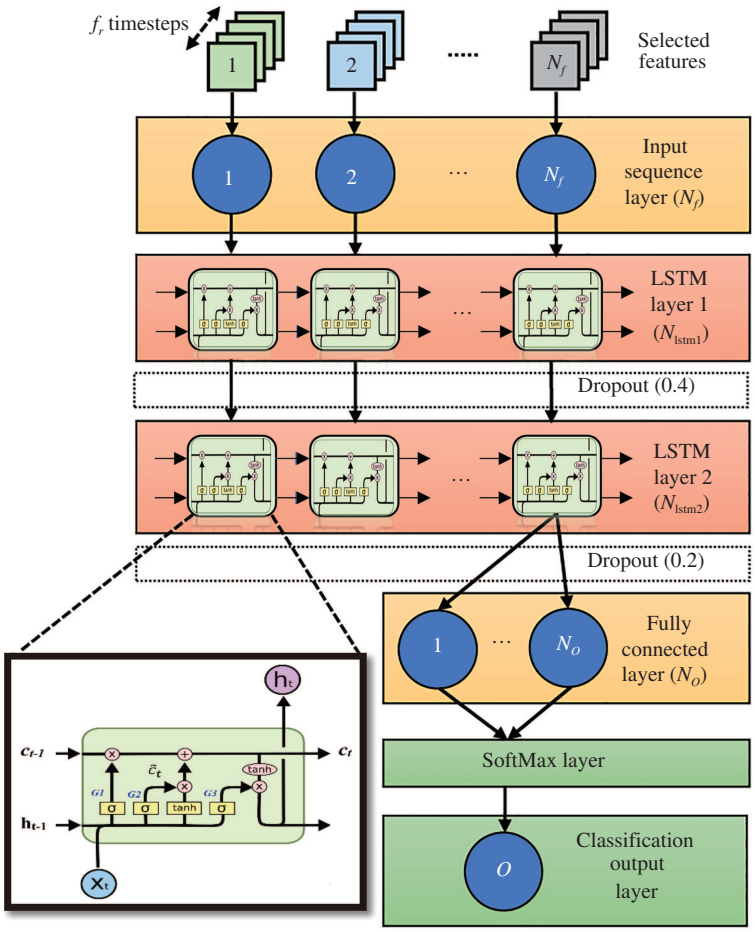

Figure 6 (Color online) The proposed classifier of the proposed system.

network based on LSTM is proposed to trace the features of each event over time and extract the temporal dependency features as shown in Figure 4. The structure of LSTM consists of five components, namely the memory cell c_t, the candidate value $\tilde{c}_t$ for updating the memory cell at each timestep, forget gate (G_1), update gate (G_2), and output gate (G_3) as shown in Figure 6. These gates are set using sigmoid functions.

Data of EEG is classified into epileptic and non-epileptic events using the 2-way classifier of the first classification level. The output epileptic waves are grouped into SPSW, GPED, and PLED events and the non-epileptic waves are classified into EYEM, ARTF, and BCKG events using the two 3-way classifiers of the second classification level. This network structure allows us to distinguish all epileptic events from the background firstly, then determines the type of epileptic event and also models the background events.

3.2.1 *Classifier structure*

The proposed classifier is shown in Figure 6 consists of eight layers, namely an input sequence layer, two cascade LSTM layers, two dropout layers, a fully connected layer, a softmax layer, and a classification output layer. The first LSTM layer has a sequence-to-sequence architecture with N_{lstm1} units, while the second LSTM layer is a sequence-to-label architecture with N_{lstm2} units. These LSTM layers are used to measure the context correlation and dependence between the timesteps of the input sequence of features (N_f). The fully connected layer is used to convert the output size of the previous layers into the number of events to classify (N_o). The softmax layer calculates the probability of each target class over all possible target classes. Finally, the classification output layer estimates the cost function to detect the target. In order to avoid the overfitting of LSTM layers, one dropout layer is added after each LSTM layer.

The classification network is trained and tested using the TUEV corpus as shown in Figure 7. The

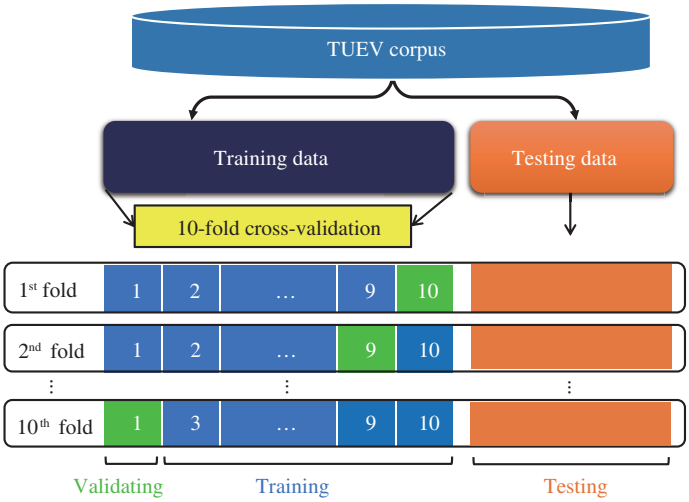

Figure 7 (Color online) Preparing data for training and testing the classification network using a 10-fold cross-validation method.

training set includes 73874 1-s epochs of six events which are grouped into an epileptic class of 11815 samples and a non-epileptic class of 62059 samples for training the 2-way classifier. Then, the epileptic data is divided into SPSW class of 645 samples, PLED class of 4120 samples, and GPED class of 7050 samples for training the first 3-way classifier. While the second 3-way classifier is trained using the three classes of the non-epileptic data, namely EYEM class of 940 samples, ARTF class of 9329 samples, and BCKG class of 51790 samples. The 10-fold cross-validation method is used for dividing the training dataset of each classifier into a training set (90%) and a validation set (10%) for training and validating the model through 10 iterations. Due to the imbalance data of different events, a resampling technique [33] is used to increase the training samples of the minority group before training the model. The training set was split into smaller training subsets during backpropagation called mini-batches to speed up the optimization algorithm. While the testing dataset described in Table 2, is used for testing the system at each iteration and the average of the obtained accuracy, sensitivity, specificity, precision, false-positive rate, F1-score, and the geometric mean for the ten iterations was taken as the final result. The adaptive moment estimation (ADAM) training algorithm was adopted for backpropagation with a maximum number of epochs is 30. The main hyperparameters used for the ADAM algorithm were: learning rate is 0.004 which is dropped out by a factor of 0.001 after every 10 epochs, decay factors of gradient and squared gradient are 0.9 and 0.999, epsilon is 10^{-8} for numerical stability and the mini-batch size is set to 256.

3.2.2 *Classifier performance*

Based on the input positive (P) and negative (N) samples to the classifier, the output will be true positive (TP), false positive (FP), true negative (TN), and false negative (FN). TP and TN are the numbers of correctly positive and negative detections respectively, FP and FN are the numbers of samples that are incorrectly detected as positive and negative respectively. The following metrics are considered depending on the outputs of the classification network to evaluate the performance of the proposed system:

• **Accuracy** (ACC $= (\mathrm{TP}+\mathrm{TN})/(\mathrm{P}+\mathrm{N})$) is the total number of correct detections divided by the total number of samples provided to the classifier.

• **Sensitivity** (SEN $= \mathrm{TP}/(\mathrm{TP}+\mathrm{FN})$) **or true positive rate** (TPR) is the total number of correct positive detections divided by the total number of positives.

• **Specificity** (SPE $= \mathrm{TN}/(\mathrm{TN}+\mathrm{FP})$) **or true negative rate** (TNR) is the total number of correct negative detections divided by the total number of negatives.

• **Precision** (PREC $= \mathrm{TP}/(\mathrm{TP}+\mathrm{FP})$) is the total number of correct positive detections divided by the total number of positive detections.

• **False positive rate** (FPR $= \mathrm{FP}/(\mathrm{TN}+\mathrm{FP}) = 1-\mathrm{SPE}$) **or false alarm rate** is the total number of false-positive detections divided by the total number of negatives.

• **F1-score** (F1-score $= 2\times(\mathrm{SEN}\times\mathrm{PREC})/(\mathrm{SEN}+\mathrm{PREC})$) is the harmonic mean of sensitivity and precision. F1-score is preferred than accuracy in the imbalanced classification case [34].

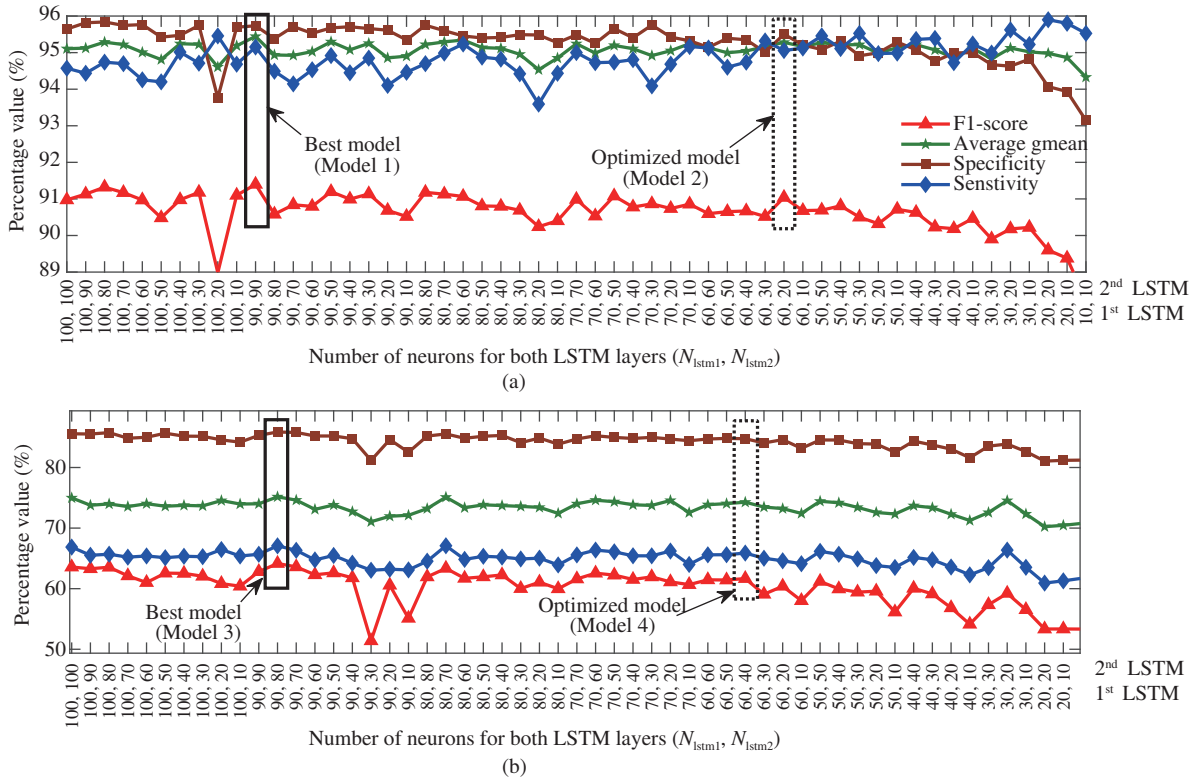

Figure 8 (Color online) Performance results for varying units of the LSTM layers. (a) 2-way classifier; (b) 3-way classifier.

• **Geometric mean** (Gmean = $\sqrt{(\text{SEN} \times \text{SPE})}$) is the square root of sensitivity and specificity. Gmean is used to measure the functionality of the proposed system due to the imbalance of the testing dataset.

3.2.3 *Classifier model optimization*

Reducing the complexity and power of the system depends on the number of features and the classification network. In order to optimize and improve the classification network, 55 networks for each classifier with different units for both the LSTM layers are developed in MATLAB (MATLAB and Neural Network Toolbox Release 2019a, The MathWorks, Inc., Natick, MA, USA). All networks have an input sequence layer with 25 neurons for the 25 significant features, that are selected using the mRMR technique, and the fully connected layer is set by 2 and 3 neurons for the 2-way and 3-way classifiers respectively. Each 1-s event is divided into 49 frames using a 40-ms window with a 50% overlap. The obtained results of the 55 networks for both classifiers are shown in Figure 8. As observed in Figure 8(a), the best results of the 2-way classifier are obtained when the units of both two LSTM layers are 90 (i.e., Model 1). These results are Gmean of 95.62%, F1-score of 91.4%, SPE of 95.68%, and SEN of 95.55%. While for the 3-way classifier, the best values of Gmean, F1-score, SPE, and SEN are 75.16%, 64.16%, 85.86%, and 67.07%, respectively, and are obtained when the units of the two LSTM layers are set to 90 and 80 respectively (i.e., Model 3), as shown in Figure 8(b).

The tradeoff between the model complexity and our target can be further optimized by selecting architectures with a small number of units that achieve the clinicians' requirements as shown by dashed boxes in Figure 8. It is observed that the optimized network (i.e., Model 2) of the 2-way classifier gives Gmean of 95.42%, F1-score of 91.17%, SPE of 95.48%, and SEN of 95.36%, when the units of the two LSTM layers are set by 60 and 20, respectively. For the 3-way classifier, results of Gmean, F1-score, SPE, and SEN are obtained by 74.28%, 61.67%, 84.74%, and 65.88% when the units of the two LSTM layers are optimized to 60 and 40 (i.e., Model 4), respectively.

Varying the number of input features has a significant effect on the performance and complexity of the system. So, 18 networks are developed for each of the 2-way and 3-way classifiers with a different number of neurons for the input layer. The units for the two LSTM layers are fixed by the previously

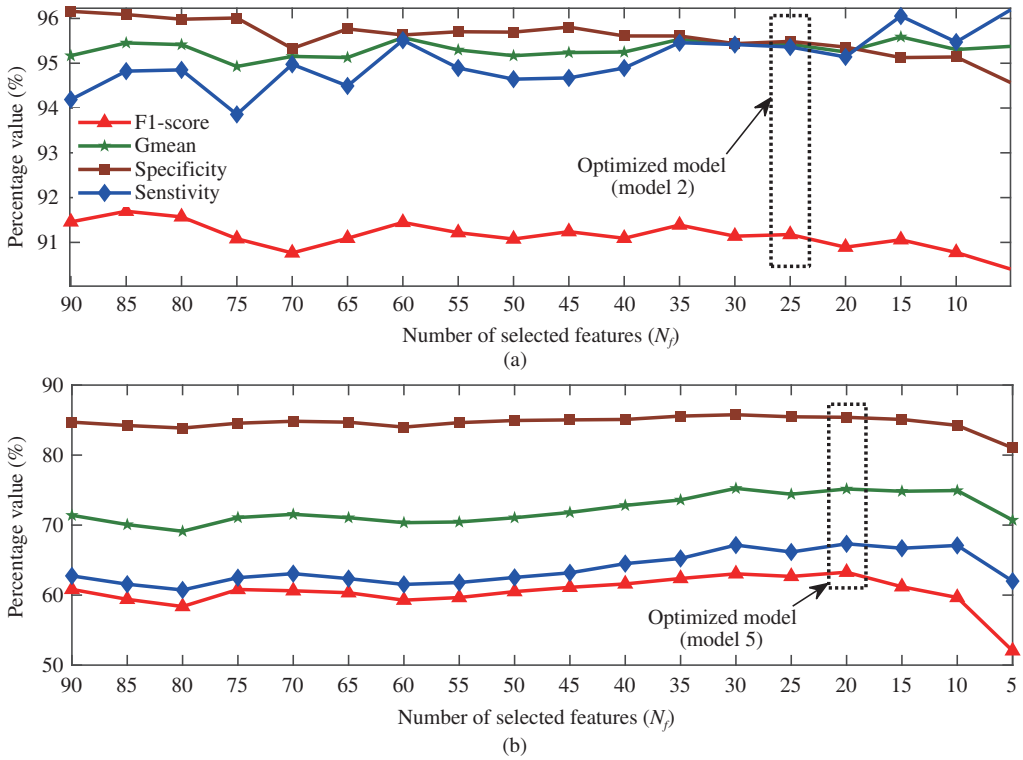

Figure 9 (Color online) Performance results for varying the neurons of the input layer. (a) 2-way classifier; (b) 3-way classifier.

Table 4 Results of the optimized models

	Classifier model				Results			
	N_f	N_{lstm1}	N_{lstm2}		Gmean (%)	F1-score (%)	SPE (%)	SEN (%)
Model 1	25	90	90	2-way classifier	95.62	91.4	95.68	95.55
Model 2	**25**	**60**	**20**		**95.42**	**91.17**	**95.48**	**95.36**
Model 3	25	90	80	3-way classifier	75.16	64.16	85.86	67.07
Model 4	25	60	40		74.28	61.67	84.74	65.88
Model 5	**20**	**60**	**40**		**75.16**	**63.27**	**85.4**	**67.33**

obtained values (60, 20) and (60, 40) for the 2-way and 3-way classifiers respectively, while the neurons of the input layer (N_f) are varied from 5 to 90 by step 5. Figure 9 shows the classifier performance against the number of neurons of the input layer for the 2-way and 3-way classifiers, respectively. It can be seen that the optimized number of neurons that achieves the clinicians' requirements is 25 neurons for the 2-way classifier and 20 neurons for the 3-way classifier.

Table 4 lists the obtained results of the best and optimized network models for the two classifiers. Note that Models 2 and 5 are the optimized models for the 2-way and 3-way classifiers. These models consist of a small number of LSTM units and neurons and give approximately the same results of models with a high number of neurons and LSTM units which lead to a low power system. The 2-way model consists of an input layer with 25 neurons, two LSTM layers with 60 and 20 units respectively, and a fully connected layer with two neurons. This model achieves Gmean of 95.42%, F1-score of 91.17%, SPE of 95.48%, and SEN of 95.36%. While the optimized model of the 3-way classifier consists of an input layer with 20 neurons, two LSTM layers with 60 and 40 units respectively, and a fully connected layer with three neurons. The obtained results of this model are Gmean of 75.1%, F1-score of 63.27%, SPE of 85.4%, and SEN of 67.33%.

To examine the informativeness of the selected features using the mRMR technique based on the degradation of the classification performance, we have replaced the value of one feature to zero while keeping the same values for the remaining features in each experiment. Thus, the experimental result is shown in Figure 10(a). The classifier performance has degraded for features #2, #12, #13, #14, #19, and #22. Furthermore, we did the opposite of the above test by considering only one feature and replacing

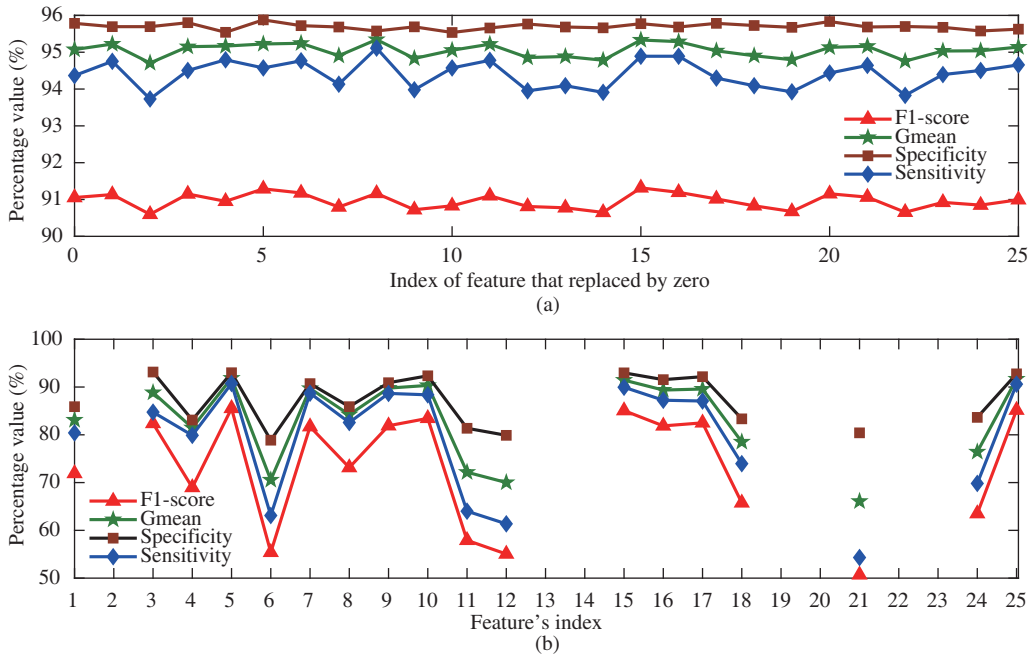

Figure 10 (Color online) Examining the informativeness of the selected features on the performance of the 2-way classifier. (a) Replacing each feature by zero; (b) considering only one feature at each case.

the remaining features by zeros in each experiment. Figure 10(b) shows the classifier performance for each feature. We observe that feature #2, #12, #14, #19, #20, #22, or #23 is not enough for the classifier, so it cannot distinguish between the epileptic and non-epileptic events. The highest sensitivity of 90.7% is occurred at the feature #5, while the lowest sensitivity of 54.3% is achieved at the feature #21. It is clear that combining the selected features by the mRMR technique can give the best performance and satisfy the clinicians' requirements. So, the mRMR technique is used here for selecting the best informative features.

4 Results and discussion

The proposed system is tested using the TUEV dataset and compared to the developed system in [8]. Since the critical issue for diagnosing epileptic seizures is detecting the epileptic discharges, the six events are grouped into epileptic (E) and non-epileptic (NE) classes. The epileptic class contains SPWS, GPED, and PLED events, while the non-epileptic class includes EYEM, ARTF, and BCKG events. Five cases are considered to study the effect of tracing features at different timesteps on the performance of the proposed system. In case 1, the 1-s epoch of each event is considered as one timestep (i.e., $f_r = 1$ and $T_w =$ 1-s). While in case 2, the 1-s epoch is divided into 4 frames to be considered as 4 timesteps (i.e., $f_r = 4$ and $T_w = 400$ ms). Cases 3 and 4 consider the 1-s event as 9 timesteps (i.e., $f_r = 9$ and $T_w =$ 200 ms) and 19 timesteps (i.e., $f_r = 19$ and $T_w = 100$ ms), respectively. Finally, in case 5 each event is divided into 49 timesteps (i.e., $f_r = 49$ and $T_w = 40$ ms) for extracting accurate features.

Table 5 shows the average of the 10-folds for the obtained validating and testing results of the 2-way classification at five cases of the proposed system compared to the results of Golmohammedi's system [8]. It is observed that increasing the timesteps for each 1-s epoch event improves the system performance from SEN of 90.86% with FPR of 9.14% in case 1 to SEN of 95.36% with FPR of 4.52% in case 5. This due to decreasing the duration of timestep that helps for extracting accurate features and allows the LSTM to track the narrow transient (20 ms) of spike waves at the different timesteps. Compared to the other systems, it is observed that cases 4 and 5 of the proposed system outperform the Golmohammedi's system. Case 5 detected 95.36 % of the IED events with an FPR of 4.52% and case 4 detected 93.81% of the IED events with an FPR of 4.63% compared to 90.1% with a 4.89% FPR of the other system [8]. This means that the proposed system with 49 timesteps improves sensitivity by 5.84% and decreases FPR by 7.57% compared to the Golmohammedi's system. Figure 11 shows the detection error tradeoff

Table 5 Results and confusion matrix of 2-way classification

Results	Proposed system N_f=25, N_{lstm1}= 60, N_{lstm2}=20										Golmohammedi's system [8]	
	Case 1 (1 timesteps)		Case 2 (4 timesteps)		Case 3 (9 timesteps)		Case 4 (19 timesteps)		Case 5 (49 timesteps)			
	Validating	Testing	Validating	Testing	Validating	Testing	Validating	Testing	Validating	Testing		
Gmean (%)	91.68	90.86	94.27	92.13	96.21	93.94	96.69	**94.59**	96.33	**95.42**	92.6	
F1-score (%)	90.47	83.04	93.42	85.92	95.58	89.17	96.14	**90.21**	95.76	**91.17**	–	
SPE (%)	91.07	90.86	94.09	93.15	95.60	94.93	96.20	**95.37**	96.21	**95.48**	95.11	
SEN (%)	92.29	90.86	94.46	91.12	96.84	92.96	97.19	**93.81**	96.44	**95.36**	90.1	
FPR (%)	8.93	9.14	5.91	6.85	4.4	5.07	3.8	**4.63**	3.79	**4.52**	4.89	
Event	**E**	**NE**	**E**	**NE**	**E**	**NE**	**E**	**NE**	**E**	**NE**	**E**	**NE**
E	**90.86**	9.14	**91.12**	8.88	**92.96**	7.04	**93.81**	6.19	**95.36**	4.64	**90.1**	9.9
NE	9.14	**90.86**	6.85	**93.15**	5.07	**94.96**	4.63	**95.37**	4.52	**95.48**	4.89	**95.11**

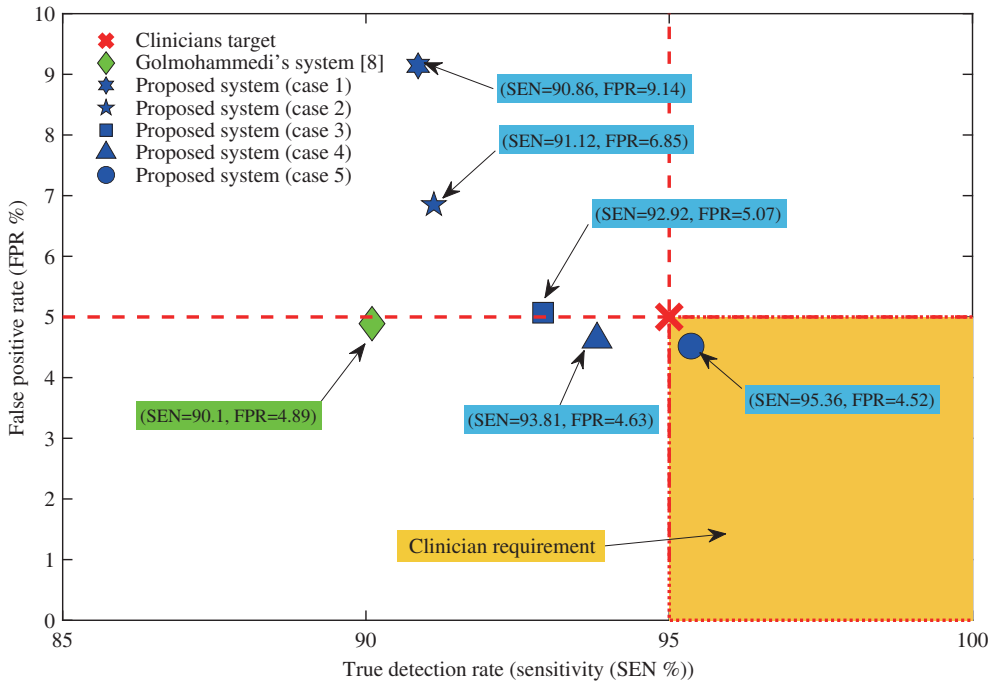

Figure 11 (Color online) DET curve of the five cases of the proposed system and the Golmohammedi's system.

curve (DET) for the two systems. It is noticed that increasing the timesteps within the 1-s epoch closes the penalty points of the proposed system toward the area of the clinicians' requirement. Case 5 of the proposed system meets the clinicians' requirements because it attained a sensitivity of 95.36% and FPR of 4.52% compared to that of the Golmohammedi's system (90.1%, 4.89%). This due to extracting features from the frequency interaction of narrow timesteps which allows the proposed system to track the transient changes of IED events. The Golmohammedi's system used a 0.9-s frame for measuring the differential energy between the maximum and minimum energy of each frame. The time frame is not sufficient to track the narrow transient changes of the IED events. According to the output of the mRMR technique, it has been seen that most of the selected 25 significant features are related to the bispectrum phase entropy, bispectrum energy, bispectrum diagonal energy, and first-order spectral moment. Moreover, $\text{WB}_{\beta\beta}$, $\text{WB}_{\beta\gamma}$, $\text{WB}_{\gamma\gamma}$, $\text{WB}_{\delta\delta}$, $\text{WB}_{\theta\alpha}$, and $\text{WB}_{\theta\beta}$ are the significant bispectrums for classifying the epileptic IED events. Figure 12 shows an example of IED detection using the proposed system of a 10-s epoch. According to the given annotation, there are four IEDs with a duration of 1-s for all 22 channels except A1-T3 and T4-A2 channels at 2.1, 3.1, 4.1, and 5.1 s. Note that our proposed system detects most of the IED events across the 22 channels of a 10-s epoch. This helps clinicians to detect IED events from the epileptic patients by counting the detected IED events and calculating the spike index [35]. The spike index for each recording is defined as the average percentage of each 1-s epoch containing the spike of epileptic discharges. Since we use a non-overlap 1-s window for segmentation, thus some FP detections have occurred when IED fall in two consecutive frames.

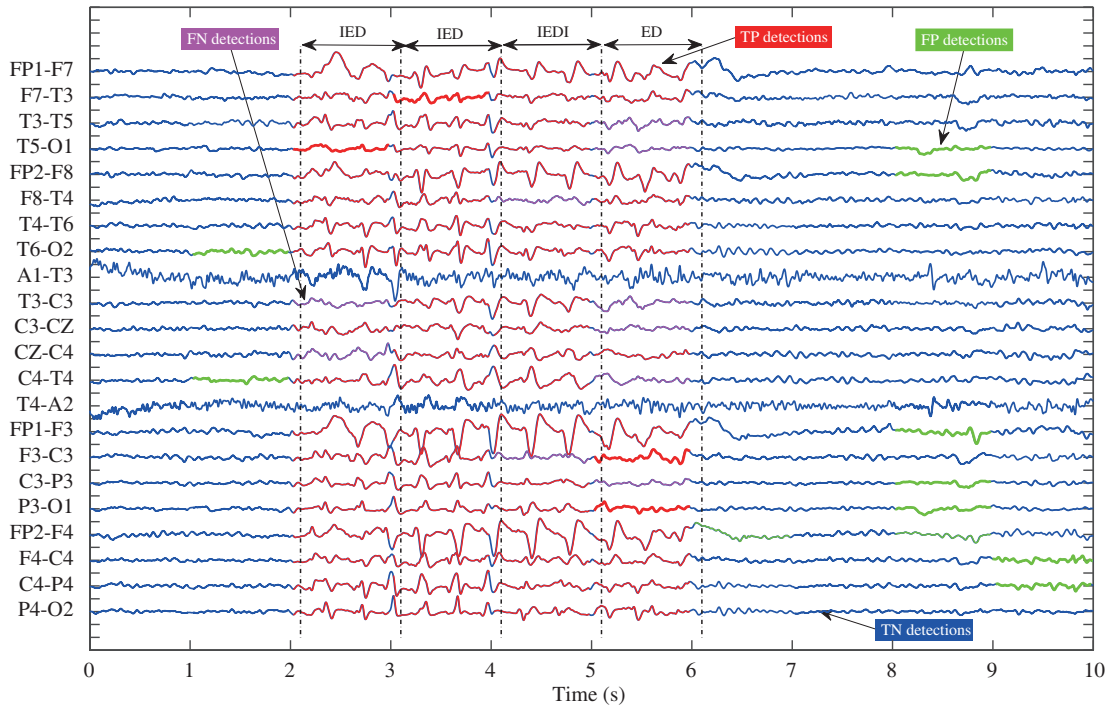

Figure 12 (Color online) Detection of IEDs for 10-s epoch of EEG recording in TUEV dataset. Red events are the TP detections, Green events are the FP detections, Pink events are the FN detections and Blue events are the TN detections.

Table 6 Classification results of the six IED events

Method	Proposed system (case 5)						Golmohammedi's system					
Event	EYEM	ARTF	BCKG	SPSW	GPED	PLED	EYEM	ARTF	BCKG	SPSW	GPED	PLED
EYEM	**89.65**	4.76	1.07				**79.31**	2.30	17.24	1.15	0	0
ARTF	0.69	**76.09**	18.70		4.52		10.18	**14.04**	72.98	2.81	0	0
BCKG	0.46	5.48	**89.54**				8.93	3.42	**81.40**	5.95	0.30	0
SPSW				**51.99**	15.49	27.88	13.33	10	33.33	**33.33**	10	0
GPED		4.64		8.16	**66.14**	21.05	0	0.3	3.65	17.63	**65.05**	13.37
PLED				13	11.72	**70.64**	0.49	0	10.76	13.69	9.78	**65.28**

In order to classify the epileptic events, the detected epileptic events of the first-level 2-way classifier are passed to the first 3-way classifier of the second classification level to be classified into SPSW, GPED, and PLED events. On the other hand, the detected non-epileptic events in the first classification level are modeled into EYEM, ARTF, and BCKG events using the second 3-way classifier of the second classification level. Table 6 lists the results of the 3-way classification of epileptic and non-epileptic for the Golmohammedi's system and case 5 of the proposed system. The obtained true detection rates using the proposed system for SPSW, GPED, and PLED are 51.99%, 66.14%, and 70.64% respectively, while those of the Golmohammedi's system are 33.33%, 65.05%, and 65.28%. It has been seen that 27.88%, and 15.49% of SPSW waves are detected as PLED and GPED respectively using the proposed system. In the other system, 33.33%, 10% and 13.33% of SPSW waves are detected as BCKG, ARTF, and EYEM events. This means that the proposed system has the ability to isolate the background events from the target epileptic events, which is the target of clinicians for diagnosing epileptic seizures.

On the other hand, the EYEM, ARTF, and BCKG events are correctly detected using the proposed system by 89.65%, 76.09%, and 89.54%, respectively compared to 79.31%, 14.04%, and 81.4% of the Golmohammedi's system. The obtained results illustrate that the interaction between frequency bands of EEG gives the ability to distinguish between different events of the EEG signal. Hence, using the LSTM network increases the robustness of the proposed system because it traces all present values in its memory to detect the spike transients and generate the target output.

According to the literature, there are many methods developed for scoring the IED of epileptic EEG recordings. Table 7 presents the comparison of the proposed method with serval research studies. It

Table 7 Comparison of the proposed system with existing methods

Method	ACC (%)	SEN (%)	SPE (%)	FPR	PREC (%)	F1-score	Gmean
Zacharaki et al. [3]	–	97	98.74	1.26%	62.8	76.24	97.87
Golmohammedi et al. [8]	–	90.1	95.11	4.89%	–	–	92.6
Carey et al. [9]	–	82.68	–	–	72.7	77.37	–
Lodder et al. [10]	–	90	–	2.36 (min)	23.10	36.76	–
Malik et al. [11]	74.1	–	–	–	–	–	–
Liu et al. [13]	93.9	95.5	92.4	7.6%	–	–	93.94
Douget et al. [14]	–	62	–	–	26	36.64	–
Antonio et al. [15]	97	86	98	2%	–	–	91.80
Proposed system	**95.45**	**95.36**	**95.48**	**4.52%**	**87.33**	**91.17**	**95.42**

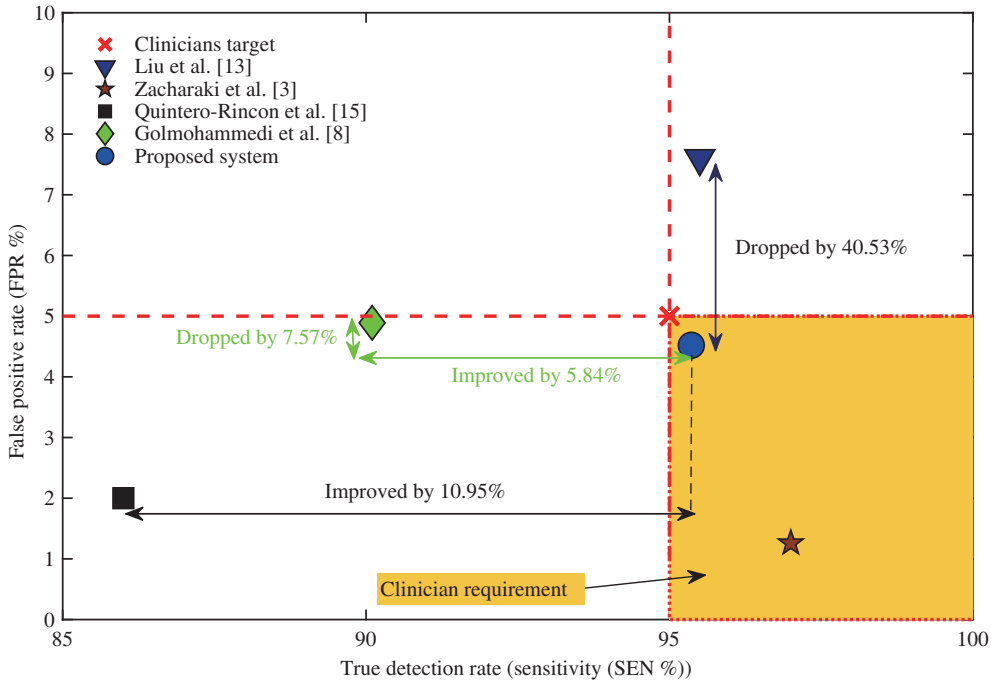

Figure 13 (Color online) DET curve of the proposed method and the existing methods.

is noted that all existing methods used their own EEG recording with a different number of subjects and channels, except the Golmohammedi's system [8] that used the EEG dataset of Temple University Hospital. It has been seen that the proposed method has the highest precision of 87.33% compared to the other methods. Figure 13 shows the DET curve for the existing developed methods. It is observed that only two methods satisfy the clinicians' requirements by gaining sensitivity more than 95% with FPR less than 5%, namely the proposed system and Zacharaki's method [3]. However, the latter method used one subject dataset compared to the largest dataset used on the proposed system as described in Table 7. Moreover, the precision and F1-score of Zacharaki's method are smaller than that are obtained using the proposed system. Compared to Golmohammedi's method that used the same TUEV dataset, the proposed system improved sensitivity by 5.84% and FPR by 7.57% which improved the Gmean by 3.05%.

For our implementation using Matlab 2019a, the proposed algorithm requires 131 ms and 164 ms using case 4 (19 timesteps) and case 5 (49 timesteps) of the proposed system on Desktop with an Intel® Core™ i5-7500 3.4 GHz processor and 16 GB RAM for detecting 1-s IED event at a sampling rate of 250 Hz. Since the durations of IED discharges are very small compared to the total time of EEG recording, the segmentation method using a moving 1-s window will increases the computational complexity and the consumption power. So in the real-time system, the nonlinear energy operator (NEO) [36, 37] and differentiation techniques are considered to identify locations of the transient changes of EEG recording and determine the candidate IED discharges as a first phase. Then, the candidate IED segments are passed to the proposed system as a second phase for classifying them into epileptic and non-epileptic

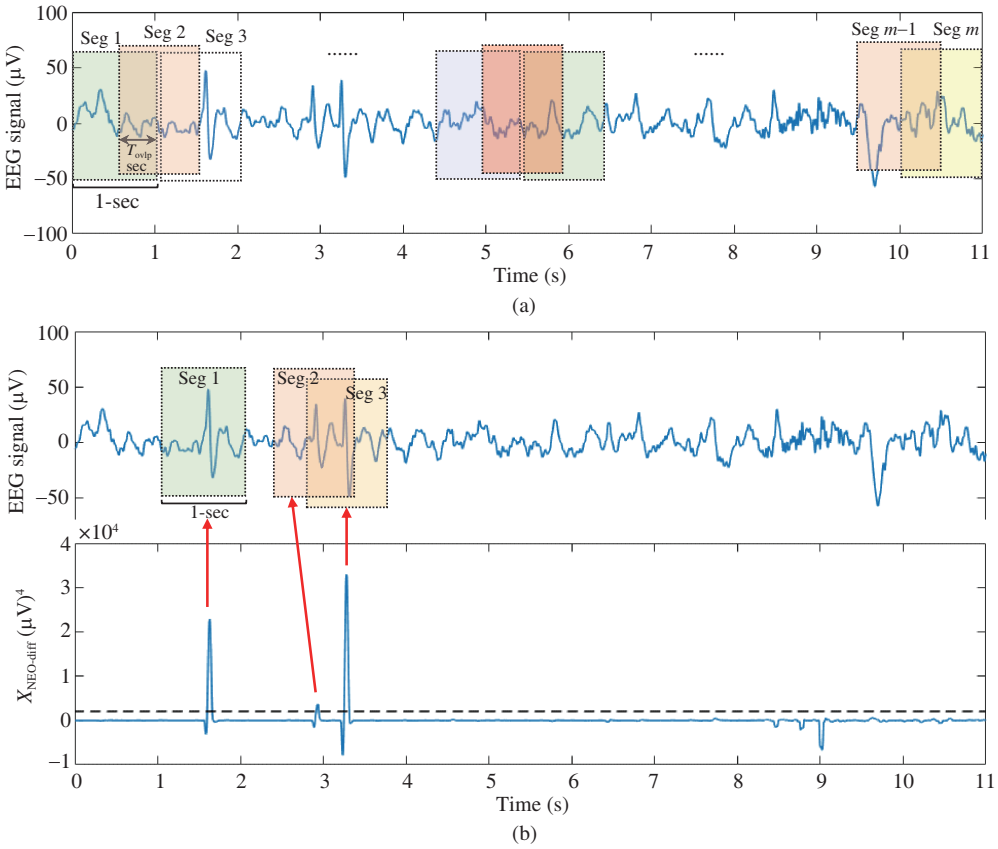

Figure 14 (Color online) Comparison between the traditional window segmentation method and the NEO-diff segmentation technique. (a) Moving Window segmentation method; (b) NEO-diff segmentation technique.

events. The locations of the candidate IED discharges are determined by finding the samples of $X_{\text{NEO-diff}}$ signal given by (15) that have amplitude larger than a threshold (thr). The value of thr depends on the mean and standard deviation of $X_{\text{NEO-diff}}$ signal as given by (18), where $C \in [0\ 1]$ is a user-defined factor.

$$X_{\text{NEO-diff}} = \text{sign}(x'(n)) \times (x'(n))^2 \times X_{\text{NEO}}, \tag{16}$$

$$X_{\text{NEO}} = x^2(n) - x(n-1)x(n+1), \tag{17}$$

$$x'(n) = x(n+1) - x(n), \tag{18}$$

$$\text{thr} = M_{X_{\text{NEO-diff}}} + C \times \text{SD}_{X_{\text{NEO-diff}}}. \tag{19}$$

Figure 14 shows an example of using the NEO method for finding the candidate IED segments compared to the traditional segmentation. The 11-s epoch of the EEG signal is segmented into 21 segments using a moving window with a 50% overlap which are passed to the proposed system for classification. On the other hand, the NEO-diff technique finds only the locations of three candidate IED segments. This means the NEO-diff technique saves the power of the system because it reduces the computational complexity by 86% compared to the moving window method. Thus, this system can be implemented as part of wearable devices for monitoring epileptic patients.

5 Conclusion

The tradeoff between the sensitivity and the false alarm rate is still a challenge for detecting the IED events. This paper proposed an automated system for detecting three types of IED events (i.e., SPSW, PLED, and GPED) and distinguishing them from three background events (i.e., EYEM, ARTF, and BCKG) based on the interaction between different frequency-bands of EEG recordings and two-level recurrent neural network. Based on the EEG dataset of Temple University Hospital, the obtained results showed that the frequency interaction between θ and α bands, θ and β bands, δ and δ bands, β and β

bands, β and γ bands, and γ and γ bands have a significant effect on detecting the IED discharges. The experimental results proved that the proposed system achieves the clinicians' requirements by detecting 95.36% of the IED events with a false-alarm rate of 4.52%. Moreover, it correctly classified the epileptic IED into SPSW, GPED, and PLED by 52.99%, 66.14%, and 70.64% respectively, and the non-epileptic waves into EYEM, ARTF, and BCKG by 89.65%, 76.09%, and 89.54% respectively. This means that the performance of the proposed system is clinically accepted and can be used to help the medical staff for making the job of the neurological experts easy. Moreover, the proposed system required only 164 ms for detecting a 1-s IED event which makes it suitable for real-time applications.

Acknowledgements This work was supported in part by National Key Research and Development Program of China (Grant No. 2019YFB2204500), National Natural Science Foundation of China (Grant No. 61874171), and Alibaba Group through Alibaba Innovative Research (AIR) Program.

References

1 de Cooman T, Varon C, van de Vel A, et al. Adaptive nocturnal seizure detection using heart rate and low-complexity novelty detection. Seizure, 2018, 59: 48–53
2 World Health Organization. Epilepsy in the Western Pacific Region: A Call to Action: Global Campaign Against Epilepsy. Manila: WHO Regional Office for the Western Pacific, 2004
3 Zacharaki E I, Mporas I, Garganis K, et al. Spike pattern recognition by supervised classification in low dimensional embedding space. Brain Inf, 2016, 3: 73–83
4 Wang S K, Pang B, Liu M, et al. A novel compression framework using energy-sensitive QRS complex detection method for a mobile ECG. Sci China Inf Sci, 2019, 62: 069409
5 Zhang Q R, Xie Q S, Duan K F, et al. A digital signal processor (DSP)-based system for embedded continuous-time cuffless blood pressure monitoring using single-channel PPG signal. Sci China Inf Sci, 2020, 63: 149402
6 Xu C Q, Liu Y, Yang Y T. An intelligent partitioning approach of the system-on-chip for flexible and stretchable systems. Sci China Inf Sci, 2018, 61: 060415
7 Bai B W, Shu H W, Wang X J, et al. Towards silicon photonic neural networks for artificial intelligence. Sci China Inf Sci, 2020, 63: 160403
8 Golmohammadi M, Harati A, de Diego S L, et al. Automatic analysis of EEGs using big data and hybrid deep learning architectures. Front Hum Neurosci, 2019, 13: 1–14
9 Carey H J, Manic M, Arsenovic P. Epileptic spike detection with EEG using artificial neural networks. In: Proceedings of International Conference on Human System Interactions (HSI), 2016. 89–95
10 Lodder S S, Askamp J, van Putten M J A M. Inter-ictal spike detection using a database of smart templates. Clin Neurophysiol, 2013, 124: 2328–2335
11 Malik M H, Saeed M, Kamboh A M. Automatic threshold optimization in nonlinear energy operator based spike detection. In: Proceedings of International Conference of IEEE Engineering in Medicine and Biology Society (EMBC), 2016. 774–777
12 Tieng Q M, Kharatishvili I, Chen M, et al. Mouse EEG spike detection based on the adapted continuous wavelet transform. J Neural Eng, 2016, 13: 026018
13 Liu Y C, Lin C C, Tsai J J, et al. Model-based spike detection of epileptic EEG data. Sensors, 2013, 13: 12536–12547
14 Douget J E L, Fouad A, Filali M M, et al. Surface and intracranial EEG spike detection based on discrete wavelet decomposition and random forest classification. In: Proceedings of International Conference of IEEE Engineering in Medicine and Biology Society (EMBC), 2017. 475–478
15 Quintero-Rincón A, Muro V, D'Giano C. Spike-and-wave detection in epileptic signals using cross-correlation and decision trees. Rev Argent de Bioingeniería, 2018, 22: 3–6
16 Assi E B, Gagliano L, Rihana S, et al. Bispectrum features and multilayer perceptron classifier to enhance seizure prediction. Sci Rep, 2018, 8: 15491
17 Chua C K, Chandran V, Acharya R, et al. Higher order spectral (HOS) analysis of epileptic EEG signals. In: Proceedings of International Conference of IEEE Engineering in Medicine and Biology Society, 2007. 6495–6498
18 Al-Kadi M, Reaz M, Ali M. Evolution of electroencephalogram signal analysis techniques during anesthesia. Sensors, 2013, 13: 6605–6635
19 Kumar D, Jadeja R, Pande S, et al. Wavelet bispectrum-based nonlinear features for cardiac murmur identification. Cogent Eng, 2018, 5: 1502906
20 Elsayed M A K. Wavelet bicoherence analysis of wind-wave interaction. Ocean Eng, 2006, 33: 458–470
21 Hadjileontiadis L J. EEG-based tonic cold pain characterization using wavelet higher order spectral features. IEEE Trans Biomed Eng, 2015, 62: 1981–1991
22 Obeid I, Picone J. The temple university hospital EEG data corpus. Front Neurosci, 2016, 10: 196
23 López S, Gross A, Yang S, et al. An analysis of two common reference points for EEGS. In: Proceedings of IEEE Signal Processing in Medicine and Biology Symposium (SPMB), 2016. 1–5
24 Esteller R, Vachtsevanos G, Echauz J, et al. A comparison of waveform fractal dimension algorithms. IEEE Trans Circ Syst I, 2001, 48: 177–183
25 Richman J S, Moorman J R. Physiological time-series analysis using approximate entropy and sample entropy. Am J Physiol-Heart Circ Physiol, 2000, 278: 2039–2049
26 Akansu A N, Haddad R A. Multiresolution Signal Decomposition. 2nd ed. San Diego: Academic Press, 2001
27 Bentley P M, McDonnell J T E. Wavelet transforms: an introduction. Electron Commun Eng J, 1994, 6: 175–186

28 Hou C, Han H, Liu Z J, et al. A wind direction forecasting method based on z-score normalization and long short-term memory. In: Proceedings of the 3rd International Conference on Green Energy and Applications (ICGEA), 2019. 172–176

29 Huang D Q, Fu Y Z, Qin N, et al. Fault diagnosis of high-speed train bogie based on LSTM neural network. Sci China Inf Sci, 2021, 64: 119203

30 Zaremba W, Sutskever I, Vinyals O. Recurrent neural network regularization. 2014. ArXiv:1409.2329

31 Bai X, Pang Y W, Zhang G F. Special focus on deep learning for computer vision. Sci China Inf Sci, 2019, 62: 220100

32 Estabrooks A, Jo T, Japkowicz N. A multiple resampling method for learning from imbalanced data sets. Comput Intell, 2004, 20: 18–36

33 Peng H C, Long F H, Ding C. Feature selection based on mutual information: criteria of max-dependency, max-relevance, and min-redundancy. IEEE Trans Pattern Anal Mach Intell, 2005, 27: 1226–1238

34 Wang S, Yao X. Multiclass imbalance problems: analysis and potential solutions. IEEE Trans Syst Man Cybern B, 2012, 42: 1119–1130

35 Reus E E M, Visser G H, Cox F M E. Determining the spike-wave index using automated detection software. J Clin Neurophysiol, 2019. doi: 10.1097/WNP.0000000000000672

36 Zarifia M H, Ghalehjogh N K, Baradaran-nia M. A new evolutionary approach for neural spike detection based on genetic algorithm. Expert Syst Appl, 2015, 42: 462–467

37 Pfammatter J A, Maganti R K, Jones M V. An automated, machine learning-based detection algorithm for spike-wave discharges (SWDs) in a mouse model of absence epilepsy. Epilepsia Open, 2019, 11: 110–122